Supporting Information

SI Text

Geologic setting of the Chañares Formation. The Triassic non-marine sedimentary record in western Argentina comprises extensional basins formed along the western margin of southern South America during the Permo-Triassic (*1–2*). One of them, the Ischigualasto-Villa Unión Basin, is extensively exposed along the border between San Juan and La Rioja provinces. The basin was filled with up to ~4000 m of predominantly alluvial, fluvial, and lacustrine deposits (Fig. SI 1). The succession begins with the Lower-Middle Triassic Talampaya and Tarjados formations, which are unconformably overlain by the Agua de la Peña Group. The Triassic strata are separated by a regional unconformity from overlying Cretaceous and Cenozoic rocks (*3–4*). The base of the Agua de la Peña Group comprises the fluvial–lacustrine tuffaceous deposits of the Chañares Formation, which is conformably overlain by the the lacustrine–fluvial black shales, siltstones, and sandstones of the Los Rastros Formation. The top of this unit is unconformable with the succeeding formation, the fluvial sandstones, mudstones, and tuffs of the Ischigualasto Formation. This unit is in turn conformably overlain by the thick fluvial "redbed" siltstone and sandstone deposits of the Los Colorados Formation (*3–4*).

At both its type locality and nearby Río Gualo (Fig. SI 2), the lower Chañares Formation consists of a fining upward succession that begins with light olive grey fine-grained sandstones (Sh, Sp) and siltstones of fluvial origin. The succession passes gradually upward into laterally persistent massive tuffaceous claystone–siltstone facies (TFm) of bluish grey color. Two discrete levels of large calcareous concretions, up to 2 m in diameter, characterize this part of the succession. The upper concretionary level is associated with a white tuffaceous siltstone layer and is devoid of fossil remains except for vertical invertebrate burrows (fig. SI 2). In contrast, the lower concretionary level contains abundant remains (Fig. SI 3), although some additional tetrapods have been also found directly embedded in the tuffaceous clay–siltstones or in small concretions within and just below the lower concretionary level (*5*). The upper part of the formation comprises grey nodular tuffaceous claystone and siltstone that are covered by greenish siltstones and sandstones of lacustrine/deltaic origin, which are overlain by the Los Rastros Formation. These uppermost greenish levels were considered part of the Los Rastros Formation by previous workers (*6*), but have been shown to be part of the Chañares

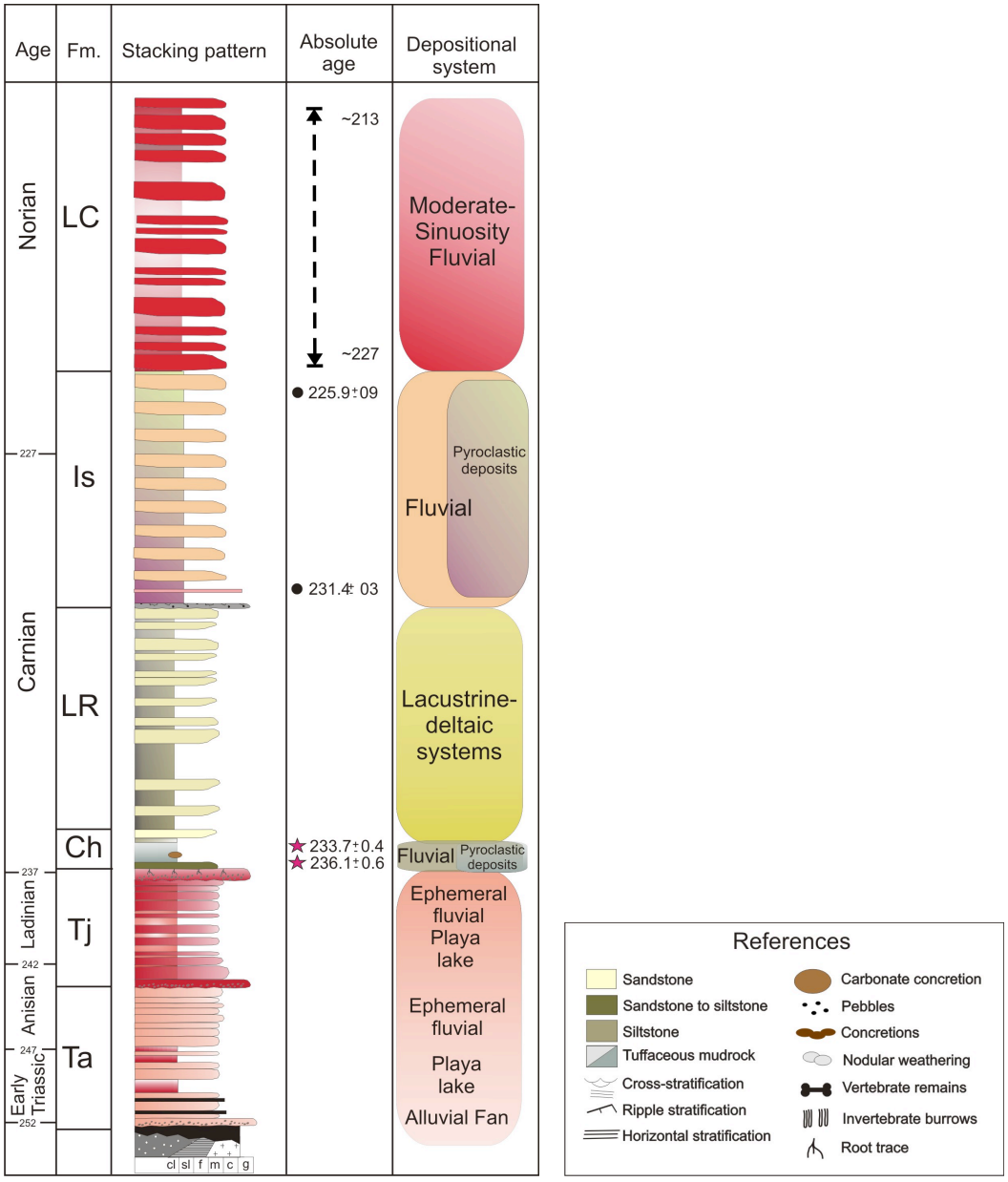

Figure SI 1. Generalized stratigraphic column of the Triassic succession in the Ischigualasto-Villa Unión Basin, with the location of previous radioisotopic and magnetostratigraphic age constraints for the Ischigualasto (*16*) and Los Colorados (*19*) formations. Ta, Talampaya Fm.; Tj, Tarjados Fm.; Ch, Chañares Fm.; LR, Los Rastros Fm.; Is, Ischigualasto Fm.; LC, Los Colorados Fm.

depositional system (*7*). The tuffaceous sandstones have been interpreted as deposited by river channels, whereas the tuffaceous claystones and siltstones represent a floodplain setting. The predominance of bedload sedimentation in the fluvial system was associated with the influx of large amounts of volcaniclastic sediment during deposition (*7*). The Chañares fossil tetrapod remains from the lower concretionary level are abundant and depict a diverse community including non-archosaur archosauromorphs (e.g., a rhynchosaur, a doswelliid, and proterochampsids), pseudosuchian archosaurs, dinosauromorphs, and therapsid synapsids (large dicynodonts and small cynodonts) (*5*–*8*).

Figure SI 2. General view of the Chañares Formation outcrops in the Río Gualo area, Talampaya National Park, La Rioja Province, Argentina.

Figure SI 3. Representative bone-bearing concretion from the fossiliferous concretionary level.

Geologic details of the dated samples. The lower of the two dated samples, RBI12/CÑ-R7, was collected from the base of the fossiliferous lower concretion level in the Río Gualo area (see Main Text Fig. 1). The sample comprises a structureless medium-sorted tan-grey siltstone that lacks bedding or any other sedimentary structures. It was collected from matrix directly associated with an associated skeleton of the traversodontid cynodont synapsid *Massetognathus pascuali* (field number M2/12, reposited in the collections of the Centro Regional de Investigaciones Científicas y Transferencia Tecnológica (CRILAR), Anillaco, La Rioja, Argentina), the quintessential tetrapod from the Chañares Formation (*9–12*), and also its most common vertebrate taxon. *M. pascuali* is important as it typifies this main bone-bearing horizon that has produced most of the vertebrate specimens of the formation, and also provides a biostratigraphic link with outcrops of the lower Santa Maria Formation in southern Brazil (*13*). Although the specimen associated with the sample was not found in a concretion, fossiliferous concretions are found a few centimeters above this level (Fig. SI 4). In the immediate vicinity, at this stratigraphic level our team has recovered fossils of dicynodonts, proterochampsids, and dinosauriforms, indicating a vertebrate assemblage nearly identical in composition to that of the type locality.

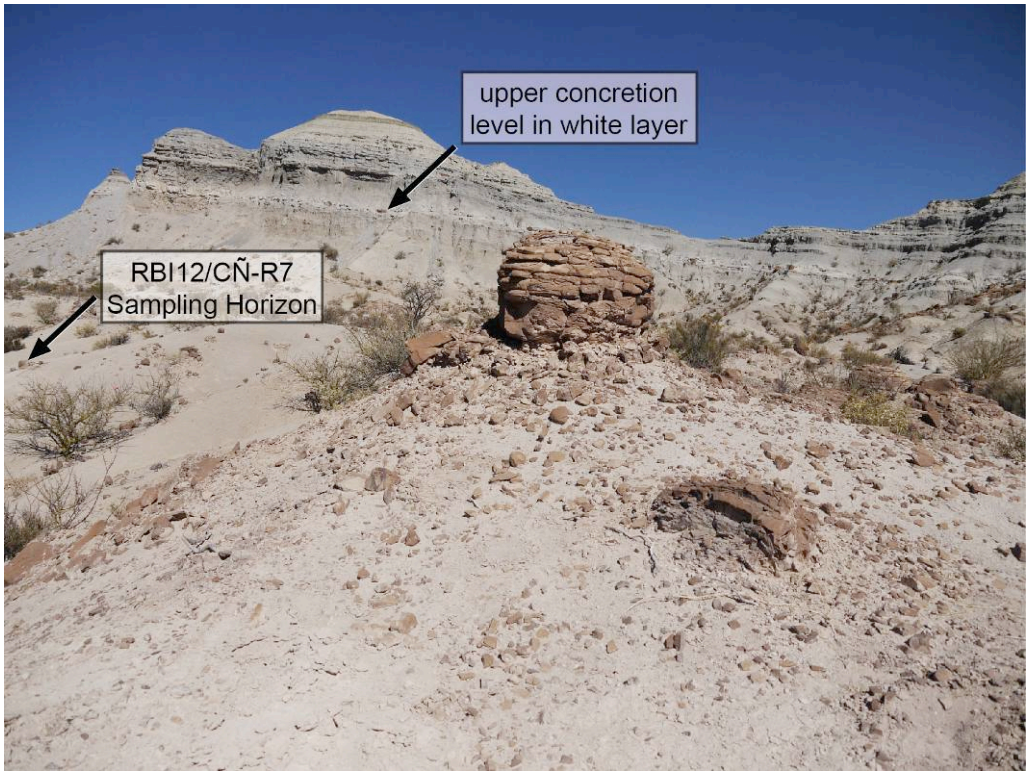

Figure SI 4. Location of the RBI12/CÑ-R7 sample at the base of the fossiliferous lower concretion level (foreground), and its relationship to the upper concretion level.

The stratigraphically-higher dated sample, Zr-11, was also collected from the Río Gualo area; it is from a horizon approximately 2 meters above the top of the non-fossiliferous upper concretion level (see Main Text Fig. 1; Figs. SI 4–SI 5). The sampled unit comprises thin (1-2 cm thick) stringers of purplish-white tuff that are complexly interbedded within a matrix of purple-grey siltstone (Fig. SI 5). These tuff layers anastomose often over lateral distances of just a few meters, but are always in the same stratigraphic horizon and position, and can be traced throughout the Río Gualo area. The tuff layers vary from having a relatively homogenous appearance to sometimes displaying a weakly brecciated fabric. We suspect it is likely that this volcanic ashfall was somewhat mixed subaqueously prior to final burial, thus resulting in its complex bedding. It is also important to note that there is no outcrop or sedimentological evidence for depositional hiatuses or unconformities in the strata between the horizons containing RBI12/CÑ-R7 and Zr-11.

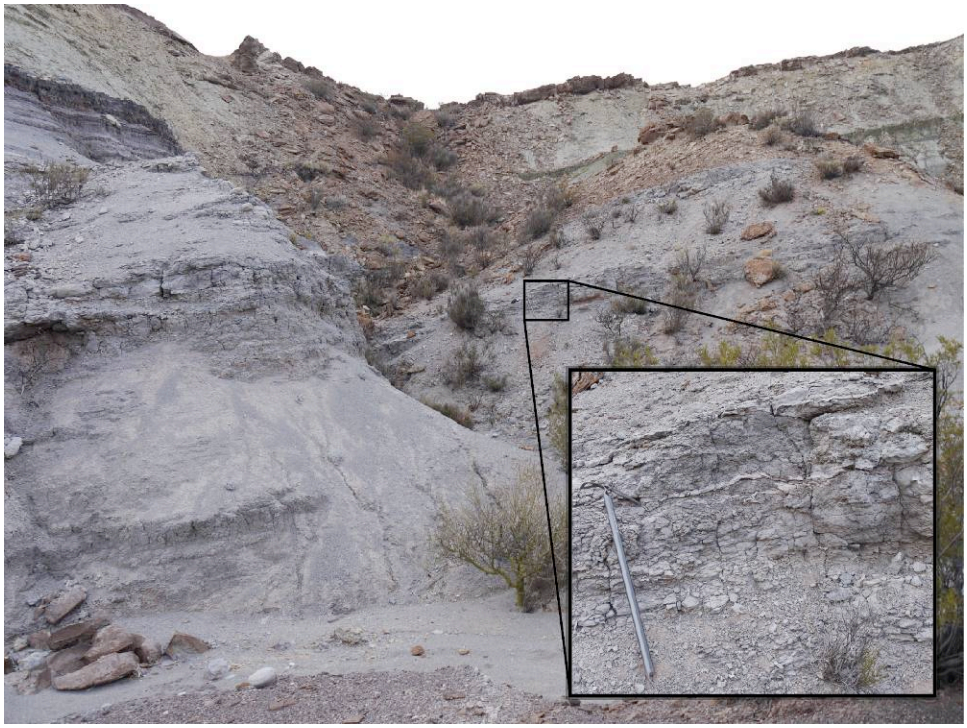

Figure SI 5. Location of Zr-11 sample (thin white bands in inset photo). Base of wash in foreground is the top of the upper concretion level.

Although the Río Gualo area has produced many fossils of classic Chañares taxa, both historically and in recent work, a large proportion of the most famous fossils are from the type locality several kilometers (~ 7.5 km) to the northwest near Río Chañares (*5*), and new discoveries are being made in outcrops to the east of these two areas (*6*). Thus, it is important to demonstrate that the dated horizons from Río Gualo can be reliably traced throughout the major fossiliferous outcrops. Our geological fieldwork confirms this is the case. In all of the major outcrop areas of the Chañares Formation in Talampaya National Park, vertebrate fossils are concentrated in a zone that is just below and within the lower concretion level, there is an unfossiliferous upper concretion level, the complexly interbedded thin white tuff (sample Zr-11) is several meters above this, and the greenish lacustrine beds cap the sequence (Fig. SI 6). Furthermore, these units maintain similar thicknesses across the outcrops. Our observations are reinforced by other recent independent geologic work, which also observed stratigraphic consistency across outcrops in the major stratigraphic units of the formation (*14*). Thus, we are

confident that our new radioisotopic ages from Río Gualo also constrain the fossiliferous horizon at the type locality and in other outcrops to the east.

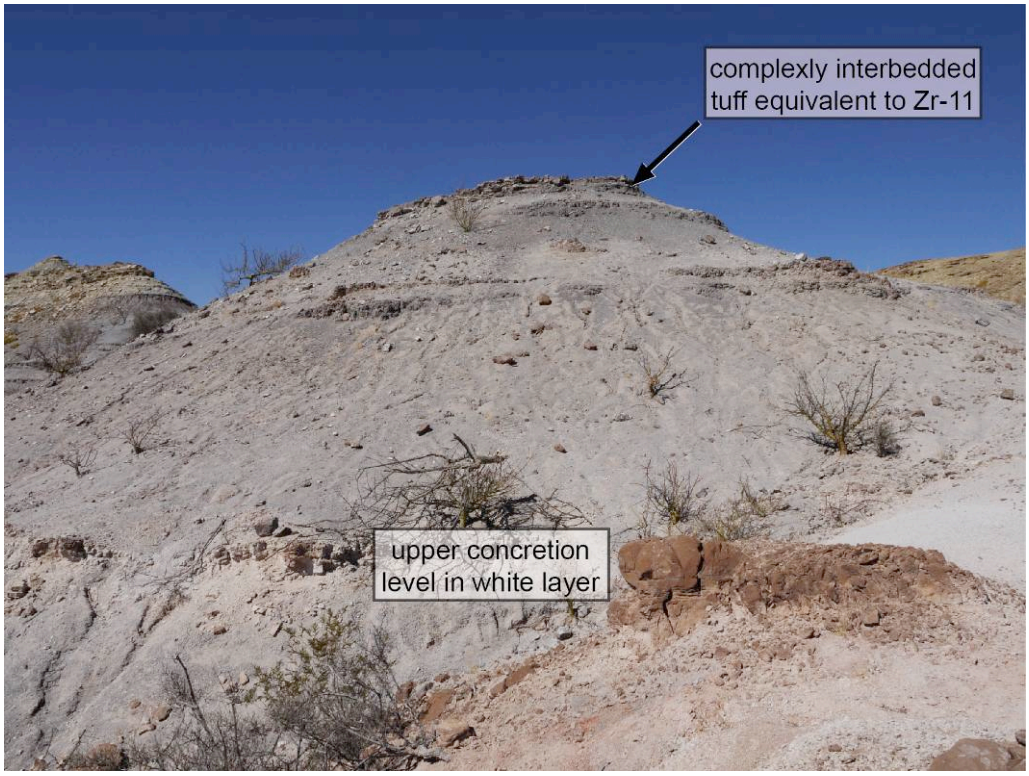

Figure SI 6. Outcrop near the type locality of the Chañares Formation demonstrating that this area shares the same stratigraphic relationships with outcrops in the Río Gualo area. Note the capping greenish lacustrine beds in the far left background of the photo.

Analytical details and results of the U-Pb zircon analyses. Zircon from samples Zr-11 and RBI12/CÑ-R7 were extracted using standard disintegration and mineral separation techniques (crusher, mill, sieves, magnetic separation, heavy liquid). Euhedral zircons where selected for analysis and mounted in epoxy for laser ablation multi-collector inductively coupled mass spectrometry (LA-ICPMS); for isotope dilution thermal ionization mass spectrometry (ID-TIMS), the crystals were thermally annealed (850°C, 48h) and chemically abraded in HF/HNO_3 (220°C, 10h) in Teflon micro capsules to remove crystal parts affected by Pb loss.

Analytical protocols (including tracer calibrations) for single zircon ID-TIMS analyses at the Berkeley Geochronology Center follow those described in Mundil et al. (*15*) and Irmis et al. (*16*). Data for ID-TIMS analyses are presented in Table S2. All individual data are analytically

concordant. Both samples show a complex age inventory due to redeposition and/or mixing, rendering calculation of a weighted mean age from an arbitrarily chosen subset unsuitable. Instead the youngest age of the population is considered a maximum age that represents the closest approximation to the depositional age of the sampled layer (see *17* for further examples of this strategy). The youngest $^{206}Pb/^{238}U$ zircon age out of 22 analyses from sample RBI12/CÑ-R7 yields 236.1 ± 0.6 Ma (Z03). The youngest $^{206}Pb/^{238}U$ zircon age out of 12 analyses from sample Zr-11 yields 233.7 ± 0.4 Ma (Z05). Th/U of the latter zircon is considerably higher than in the remaining analyses of Zr-11 zircons lending further evidence for the presence of multiple subpopulations from different sources in that sample. Alternatively, since its age is not reproduced, the young age of Z05 may be due to Pb loss in which case an age of 235.1 ± 0.5 Ma (Z63), which is reproduced by 2 ages (Z03, Z64), may be considered the maximum depositional age for Zr-11. In absence of additional age constraints from younger layers with unambiguous stratigraphic context, even the assignment of a maximum age for Zr-11 is fragile; however, we caution against ignoring a resolved younger age since it can truly represent an accurate age of an

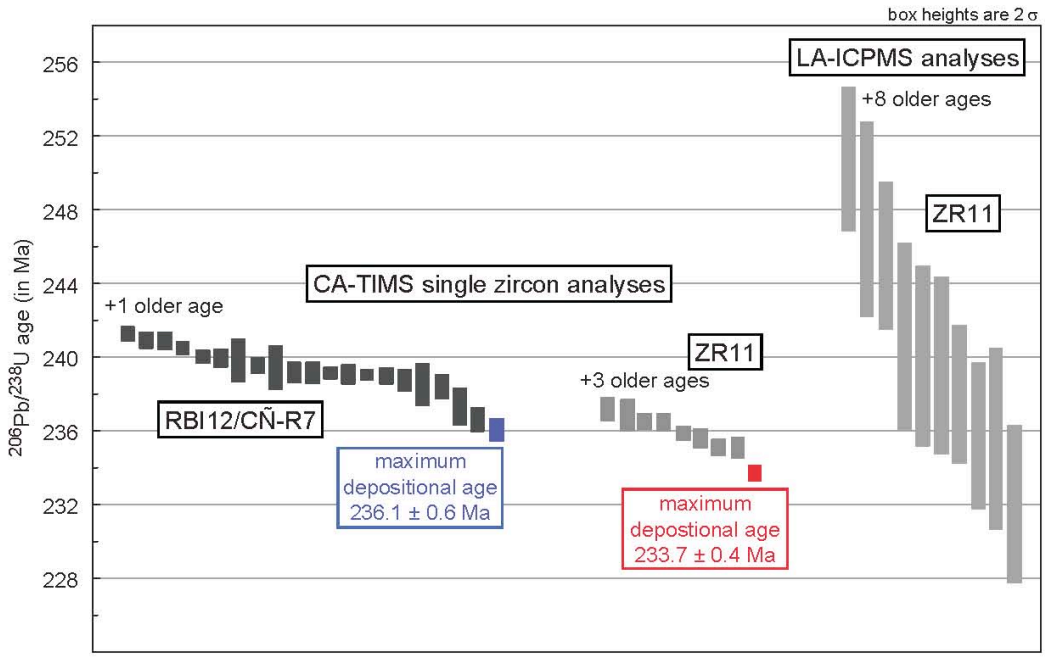

underrepresented subpopulation (*18, 19*). Prior to ID-TIMS analyses, in situ U-Pb isotopic measurements were performed on zircons from Zr-11 by the LA-ICPMS method.

Figure SI 7. Age ranked ID-TIMS and LA-ICPMS dates and interpreted maximum ages.

The analyses revealed the presence of multiple zircon sub populations within this layer which called for the application of superior analytical resolution. For these in situ analyses a Thermo Finnigan Neptune multicollector-ICPMS and a Nd:YAG UP213 New Wave laser ablation system at the Geochronology Laboratory of Universidade Federal do Rio Grande do Sul was used. The analytical procedures follow the methods presented by Chemale et al. (*20, 21*). U-Pb isotope data were acquired in static mode with spot sizes of 25 and 40 μm. Laser-induced elemental fractional and instrumental mass discrimination were corrected using the reference zircon GJ-1 (*22*). To evaluate the accuracy and precision of the laser-ablation results, we analyzed an internal standard, the Temora 2. The external error was calculated after the propagation error of the GJ-1 mean and the individual sample zircon (or spot). The reproducibility obtained from the GJ-1 was 0.78% for $^{207}Pb/^{206}Pb$ and 1.3% for $^{206}Pb/^{238}U$ ratios. The individual errors of juvenile zircon grains obtained during the analyses for $^{206}Pb/^{238}U$ ratio were usually between 0.8% and 2.9 %. Isoplot 3 software was used for the final age calculations and construction of diagrams and relative probability plots (*23*). The U-Pb zircon data are presented in Table S3. The youngest LA-ICPMS zircon analysis from Zr-11 yields an age of 232.0 ± 4.3 Ma which is in agreement with, but less precise than, the maximum age inferred from ID-TIMS analyses (see above)

Data and data sources for main text Figure 3. The Middle-Upper Triassic formations of the Ischigualasto-Villa Unión Basin on the x-axis of Figure 3 are scaled to time (not stratigraphic thickness) based on the age constraints reported in this paper, and those of Martínez et al. (*24*) and Kent et al. (*25*). Paleoecological values were calculated as a proportion of the total number of species or specimens in a given tetrapod assemblage (see Table SI 1). Data for the Chañares Formation were taken from Mancuso et al. (*26*) with the addition of the new occurrence in Ezcurra et al. (*6*). Data for the lower Ischigualasto Formation were derived from Martínez et al. (*27*). We restricted the data for this bin to that from the lower third of the formation (the *Scaphonyx-Exaeretodon-Herrerasaurus* biozone), because including all occurrences for the formation would bias the dataset as it would time-average over a ~5-million year interval. Furthermore, we did not include the *Exaeretodon* or *Jachaleria* biozones as datapoints, because of their very small sample sizes. Los Colorados Formation data were taken from the compilation

in the Supplementary Information of Irmis et al. (*16*), but updated with the occurrences in Ezcurra and Apaldetti (*28*) and Apaldetti et al. (*29*). These data exclude *Jachaleria* specimens from the base of the formation (all others are from the upper third of the formation), for the same time-averaging reason.

1. Uliana MA, Biddle KT, Cerdan J (1989) Mesozoic extension and the formation of Argentine sedimentary basins. *AAPG Memoir* 46: 599-614.
2. Spalletti LA (1999) Cuencas Triásicas del sudoeste Argentino: origen y evolución. *Acta Geológica Hispanica* 32: 29-50.
3. Milana JP, Alcober, O (1994) Modelo tectosedimentario de la cuenca triásica de Ischigualasto (San Juan, Argentina). *Rev. Asoc. Geol. Arg*. 49: 217-235.
4. Caselli AT, Marsicano CA, Arcucci AB (2001) Sedimentología y paleontología de la Formación Los Colorados, Triásico Superior (provincias de La Rioja y San Juan, Argentina). *Rev. Asoc. Geol. Arg*. 56: 173–188.
5. Romer AS, Jensen J (1966) The Chañares (Argentina) Triassic reptile fauna. II. Sketch of the geology of the Rio Chañares, Rio Gualo region *Breviora* 252: 1–20.
6. Ezcurra MD et al. (2014) The oldest rhynchosaur from Argentina: a Middle Triassic rhynchosaurid from the Chañares Formation (Ischigualasto-Villa Unión Basin, La Rioja Province). *Paläontologische Zeitschrift* 88: 453-460.
7. Mancuso AC, Caselli AT (2012) Paleolimnology evolution in rift basins: the Ischigualasto-Villa Unión Basin (central-western Argentina) during the Triassic. *Sedimentary Geology* 275-276: 38-54.
8. Marsicano CA, Gallego O, Arcucci AB (2001) Faunas del Triásico: relaciones, patrones de distribución y sucesión temporal. *El Sistema Triásico en Argentina*, eds. Morel E, Artabe A, Zammuner A (Fund. Mus. La Plata, La Plata), pp. 147–157.

9. Romer AS (1967) The Chañares (Argentina) Triassic reptile fauna. III. Two new gomphodonts, *Massetognathus pascuali* and *M. teruggii*. *Breviora* 264:1-25.
10. Romer AS (1972) The Chañares (Argentina) Triassic reptile fauna. XVII. The Chanares gomphodonts. *Breviora* 396:1-9.
11. Jenkins Jr. FA (1970) The Chañares (Argentina) Triassic reptile fauna. VII. The postcranial skeleton of the traversodontid Massetognathus pascuali (Therapsida, Cynodontia). *Breviora* 352:1-28.
12. Abdala FN, Giannini NP (2000) Gomphodont cynodonts of the Chañares Formation: the analysis of an ontogenetic sequence. *J. Vert. Paleo*. 20: 501-506.
13. Liu J, Soares MB, Reichel M (2008) *Massetognathus* (Cynodontia, Traversodontidae) from the Santa Maria Formation of Brazil. *Rev. Bras. Paleont*. 11: 27-36.
14. Fiorelli LE, et al. (2013) The oldest known communal latrines provide evidence of gregarism in Triassic megaherbivores *Nature Scientific Reports* 3: 1-7.
15. Mundil R, Ludwig KR, Metcalfe I, Renne PR (2004) Age and timing of the Permian mass extinctions: U/Pb dating of closed-system zircons. *Science* 305:1760-1763.
16. Irmis RB, Mundil R, Martz JW, Parker WG (2011) High-resolution U–Pb ages from the Upper Triassic Chinle Formation(New Mexico, USA) support a diachronous rise of dinosaurs. *Earth Planet. Sc. Lett*. 309: 258-267.
17. Schoene B et al. (2010) Correlating the end-Triassic mass extinction and flood basalt volcanism at the 100 ka level. *Geology* 38: 387-390.
18. Barrett PM et al. (2014) A palaeoequatorial ornithischia and new constraints on early dinosaur diversification. *Proc. Royal Soc. London, B. Sc.* 281: 1-6.

19. Langer MC et al. (2014) New dinosaur (Theropoda, stem-Averostra) from the earliest Jurassic of the La Quinta formation, Venezuelan Andes. *Royal Society Open Science* 1: 1-13.

20. Chemale Jr. F et al. (2011) Lu-Hf and U-Pb age determination of Capivarita Anorthosite in the Dom Feliciano Belt, Brazil. *Precambrian Research* 186: 117-126.

21. Chemale Jr. F et al. (2012) U-Pb zircon in situ dating with LA-MC-ICP-MS using a mixed detector configuration. *An. Acad. Bras. Cs*. 84: 275-295.

22. Jackson SE, Pearson NJ, Griflin WL, Belousova EA (2004) The application of laser ablation-inductively coupled plasma-mass spectrometry to in situ U–Pb zircon geochronology. *Chemical Geology* 211: 47-69.

23. Ludwig KR (2003) *Using Isoplot/Ex, version 3.00* (Berkeley Geoc. Cent. Sp. Pub. No. 1).

24. Martinez RN et al. (2011) A basal dinosaur from the dawn of the dinosaur era in southwestern Pangaea. *Science* 331: 206-210.

25. Kent DV, Santi Malnis P, Colombi CE, Alcober OA, Martínez RN (2014) Age constraints on the dispersal of dinosaurs in the Late Triassic from magnetochronology of the Los Colorados Formation (Argentina). *Natl. Acad. Sc*. 111: 7958-7963.

26. Mancuso AC, Gaetano LC, Leardi JM, Abdala FN, Arcucci AB (2014) The Chañares Formation: a window to a Middle Triassic tetrapod community. *Lethaia* 47: 244-265.

27. Martínez RN et al. (2013) Vertebrate succession in the Ischigualasto Formation. *Soc. Vert. Pal. Memoir* 12:10-30.

28. Ezcurra MD, Apaldetti C (2012) A robust sauropodomorph specimen from the Upper Triassic of Argentina and insights on the diversity of the Los Colorados Formation. *Geol. Assoc*. 123: 155-164.

29. Apaldetti C, Pol D, Yates A (2013) The postcranial anatomy of *Coloradisaurus brevis* (Dinosauria: Sauropodomorpha) from the Late Triassic of Argentina and its phylogenetic implications. *Palaeontology* 56: 277-301.
30. Stacey JS, Kramers JD (1975) Approximation of terrestrial lead isotope evolution by a two-stage model. *Earth and Planetary Science Letters* 26: 207-221.

Supporting Tables

Table S1

Chañares Formation

	Species	*% of Total*	Specimens	*% of Total*
Dinosauria	0	0	0	0
Dinosauromorpha	4	25	15	4.40
Archosauriformes	10	62.5	62	18.18
Synapsida	5	31.25	278	81.52
Total Vertebrates	16		341	

Ischigualasto Formation

	Species	*% of Total*	Specimens	*% of Total*
Dinosauria	5	20.83	79	10.35
Dinosauromorpha	7	29.17	82	10.75
Archosauriformes	13	54.17	138	18.09
Synapsida	8	33.33	168	22.02
Total Vertebrates	24		763	

Los Colorados Formation

	Species	*% of Total*	Specimens	*% of Total*
Dinosauria	5	38.46	27	36.49
Dinosauromorpha	5	38.46	27	36.49
Archosauriformes	10	76.92	41	55.41
Synapsida	2	15.38	3	4.05
Total Vertebrates	13		74	

Table S1. Paleoecological data for Main Text Figure 3 from the Ischigualasto-Villa Unión Basin of northwestern Argentina.

Table SI 2.

			isotopic ratios								age in Ma	
Sample	Pb_c [a] (pg)	Th [b] U	^{206}Pb [c] / ^{204}Pb	^{207}Pb [d] / ^{206}Pb	2s %	^{207}Pb [d] / ^{235}U	2s %er	^{206}Pb [d] / ^{238}U	2s %	r [e]	^{206}Pb* / ^{238}U	
RBI12CNR7.Z39	0,6	0,90	1788	0,05189	0,35	0,3088	0,47	0,043165	0,29	,66	272,42	± 0,78
RBI12CNR7.Z40	0,6	1,07	582	0,05141	1,16	0,2704	1,22	0,038139	0,16	,42	241,29	± 0,39
RBI12CNR7.Z41	0,6	0,91	5206	0,05102	0,25	0,2679	0,32	0,038083	0,18	,62	240,94	± 0,42
RBI12CNR7.Z32	0,4	0,42	4396	0,05111	0,31	0,2684	0,38	0,038080	0,19	,56	240,92	± 0,45
RBI12CNR7.Z07	0,5	0,78	1843	0,05116	0,79	0,2682	0,82	0,038017	0,14	,29	240,53	± 0,33
RBI12CNR7.Z02	0,9	1,02	966	0,05130	0,67	0,2683	0,71	0,037940	0,14	,39	240,05	± 0,33
RBI12CNR7.Z36	1,8	0,74	641	0,05120	0,98	0,2678	1,04	0,037928	0,20	,39	239,98	± 0,47
RBI12CNR7.Z06	1,2	1,15	303	0,05161	5,63	0,2698	5,98	0,037909	0,47	,76	239,86	± 1,13
RBI12CNR7.Z42	0,7	0,80	661	0,05106	0,99	0,2666	1,05	0,037867	0,18	,40	239,60	± 0,42
RBI12CNR7.Z28	0,9	1,09	139	0,05236	6,05	0,2732	6,35	0,037847	0,48	,64	239,48	± 1,16
RBI12CNR7.Z38	0,6	1,01	1801	0,05101	0,37	0,2659	0,45	0,037804	0,23	,57	239,21	± 0,54
RBI12CNR7.Z21	0,7	1,08	299	0,05010	2,57	0,2611	2,70	0,037799	0,24	,58	239,17	± 0,56
RBI12CNR7.Z33	0,5	0,88	3004	0,05074	0,30	0,2644	0,34	0,037795	0,13	,50	239,15	± 0,31
RBI12CNR7.Z37	0,7	1,34	515	0,05137	1,34	0,2677	1,42	0,037788	0,22	,42	239,11	± 0,52
RBI12CNR7.Z35	0,5	0,89	1026	0,05120	0,64	0,2667	0,68	0,037785	0,12	,40	239,09	± 0,29
RBI12CNR7.Z08	0,4	1,04	1578	0,05119	0,55	0,2666	0,60	0,037775	0,18	,45	239,02	± 0,42
RBI12CNR7.Z04	0,6	1,26	694	0,05097	1,09	0,2652	1,16	0,037735	0,25	,40	238,78	± 0,60
RBI12CNR7.Z22	0,7	1,17	155	0,05268	5,94	0,2738	6,25	0,037696	0,48	,66	238,53	± 1,14
RBI12CNR7.Z34	0,5	1,00	1254	0,05120	0,52	0,2660	0,60	0,037682	0,27	,53	238,45	± 0,64
RBI12CNR7.Z31	0,5	1,07	3292	0,05107	0,29	0,2641	0,52	0,037507	0,42	,83	237,36	± 1,00
RBI12CNR7.Z01	0,5	1,25	1791	0,05135	0,80	0,2647	0,85	0,037391	0,27	,35	236,64	± 0,65
RBI12CNR7.Z03	0,9	1,86	478	0,05131	1,60	0,2639	1,69	0,037302	0,25	,44	236,09	± 0,58
ZR11.Z05	1,3	0,49	1627	0,05696	0,49	0,6019	0,94	0,076644	0,78	,85	476,06	± 3,72
ZR11.Z68	1,4	0,52	436	0,05292	1,43	0,3657	1,50	0,050121	0,21	,42	315,26	± 0,65
ZR11.Z10	1,4	0,50	191	0,05223	6,03	0,3233	6,39	0,044889	0,48	,76	283,06	± 1,37
ZR11.Z61	0,8	0,92	561	0,05121	1,35	0,2647	1,42	0,037483	0,26	,33	237,21	± 0,61
ZR11.Z67	0,9	0,96	188	0,05106	3,93	0,2635	4,12	0,037425	0,36	,55	236,85	± 0,86
ZR11.Z65	0,8	0,88	505	0,05133	1,31	0,2645	1,38	0,037372	0,17	,45	236,52	± 0,41
ZR11.Z62	1,5	1,03	854	0,05104	0,81	0,2630	0,87	0,037364	0,21	,41	236,47	± 0,49
ZR11.Z69	0,6	0,79	428	0,05159	1,49	0,2651	1,56	0,037266	0,16	,48	235,86	± 0,38
ZR11.Z03	1,2	0,85	427	0,05156	1,62	0,2646	1,70	0,037224	0,22	,44	235,60	± 0,51
ZR11.Z64	0,8	0,92	747	0,05119	0,94	0,2622	1,00	0,037143	0,18	,40	235,10	± 0,42
ZR11.Z63	1,5	0,69	612	0,05135	1,20	0,2629	1,27	0,037140	0,23	,39	235,08	± 0,54
ZR11.Z08	1,5	1,60	475	0,05104	1,46	0,2598	1,53	0,036918	0,17	,46	233,70	± 0,41

a) total common Pb including analytical blank
Blank composition is $^{206}Pb/^{204}Pb$ = 18.35 ± 0.46, $^{207}Pb/^{204}Pb$ = 15.60 ± 0.32, $^{208}Pb/^{204}Pb$ = 37.95 ± 0.85 (all 2σ of population), and a $^{206}Pb/^{204}Pb$-$^{207}Pb/^{204}Pb$ correlation of +0.59
b) present day Th/U ratio calculated from radiogenic $^{208}Pb/^{206}Pb$ and age
c) measured value corrected for tracer contribution and mass fractionation (0.15 ± 0.06 %/amu)
d) ratios of radiogenic Pb versus U; data corrected for mass fractionation, tracer contribution and common Pb contribution
e) correlation coefficient of radiogenic $^{207}Pb/^{235}U$ versus $^{206}Pb/^{238}U$
Uncertainties of individual ratios and ages are given at the 2s level and do not include decay constant errors.
Ratios involving ^{206}Pb are corrected for initial disequilibrium in $^{230}Th/^{238}U$ adopting Th/U=3.6 for the crystallization environment.
Ages in grey boxes are interpreted as maximum depositonal age.

Table SI 3

Spot Number	f_{206}[a]	Pb ppm	Th ppm	U ppm	Th/U[b]	Isotope ratios[c] $^{207}Pb/^{235}U$	1 σ [%]	$^{206}Pb/^{238}U$	1 σ [%]	Rho[d]	$^{207}Pb/^{206}Pb$[e]	1 σ [%]	Ages (Ma) $^{206}Pb/^{238}U$	2 σ abs
I-IX-04	0,0002	34	45	133	0,34	1,9785	2,86	0,1900	0,36	0,13	0,0755	2,84	1121	8
I-IX-01	0,0001	17	34	174	0,20	0,6234	3,66	0,0794	0,53	0,15	0,0570	3,62	492	5
H-VIII-06	0,0000	14	71	176	0,41	0,6073	2,60	0,0780	0,69	0,27	0,0564	2,51	484	7
I-IX-16	0,0002	9	49	84	0,59	0,6022	3,85	0,0777	0,53	0,14	0,0562	3,82	482	5
H-VIII-29	0,0001	11	81	178	0,46	0,3695	9,68	0,0519	3,72	0,38	0,0516	8,94	326	24
H-VIII-46	0,0003	3	34	49	0,71	0,2696	35,30	0,0450	2,44	0,07	0,0434	35,22	284	14
I-IX-06	0,0001	20	276	289	0,96	0,3065	4,70	0,0435	0,62	0,13	0,0511	4,65	275	3
H-VIII-23	0,0001	6	68	89	0,76	0,2829	14,29	0,0432	0,90	0,06	0,0475	14,26	273	5
H-VIII-13	0,0002	7	167	143	1,17	0,2801	11,64	0,0397	0,79	0,07	0,0512	11,62	251	4
H-VIII-02	0,0000	12	317	238	1,34	0,2762	3,01	0,0391	1,09	0,36	0,0512	2,80	247	5
H-VIII-16	0,0001	25	483	614	0,79	0,2731	4,41	0,0388	0,83	0,19	0,0510	4,33	245	4
H-VIII-03	0,0006	22	453	398	1,15	0,2759	3,15	0,0381	1,07	0,34	0,0525	2,97	241	5
H-VIII-05	0,0000	6	148	100	1,49	0,2701	3,94	0,0379	1,04	0,26	0,0516	3,80	240	5
H-VIII-33	0,0002	6	81	92	0,88	0,2641	6,65	0,0379	1,02	0,15	0,0506	6,57	240	5
H-VIII-10	0,0001	15	358	348	1,04	0,2675	3,83	0,0376	0,80	0,21	0,0516	3,75	238	4
H-VIII-21	0,0004	6	129	131	0,99	0,2615	5,27	0,0372	0,85	0,16	0,0509	5,20	236	4
H-VIII-08	0,0000	15	503	228	2,22	0,2597	3,72	0,0372	1,06	0,28	0,0506	3,57	236	5
H-VIII-12	0,0001	9	163	238	0,69	0,2555	5,71	0,0366	0,94	0,16	0,0506	5,64	232	4

[a]Fraction of the non-radiogenic ^{206}Pb in the analyzed zircon spot, where f_{206}=[$^{206}Pb/^{204}Pb$]c/[$^{206}Pb/^{204}Pb$]s (c=common; s=sample)
[b]Th/U ratios and amount of Pb, Th and U (in pmm) are calculated relative to 91500 reference zircon
[c] Corrected for background and within-run Pb/U fractionation and normalised to reference zircon GJ-1 (ID-TIMS values/measured value); $^{207}Pb/^{235}U$ calculated using ($^{207}Pb/^{206}Pb$)/($^{238}U/^{206}Pb$ * 1/137.88)
[d]Rho is the error correlation defined as the quotient of the propagated errors of the $^{206}Pb/^{238}U$ and the $^{207}/^{235}U$ ratio
[e]Corrected for mass-bias by normalising to GJ-1 reference zircon and common Pb using the model Pb composition of (*59*)